Polymer luminescent concentrators containing oxide nanocrystals doped with rare-earth elements matched to an edge-illuminated silicon solar cell

Jerzy Sarnecki[1], Grzegorz Gawlik[1], Ludwika Lipińska[1], Olgierd Jeremiasz[2]
[1] Institute of Electronic Materials Technology,
133 Wolczynska Str., 01-919 Warsaw, POLAND
e-mail: Jerzy.Sarnecki@itme.edu.pl

[2] ABRAXAS,
27 Piaskowa Str., 44-300 Wodzisław Śląski, POLAND

Abstract: Luminescent Solar Concentrators (LSCs) suitable to work in conjunction with a new type of a silicon epitaxial edge-illuminated solar cell (EISC) are developed, and the operating principle of epitaxial EISCs and their specific properties are explained and discussed. The potential application of active composite materials based on luminescent nanocrystals dispersed in a polymer matrix (PMMA) in the LSCs technology is shown. The results of the synthesis of the transparent material by the incorporation of the clusters of co-doped Nd and Yb yttrium aluminum garnet $Y_3Al_5O_{12}$ (YAG), gadolinium gallium garnet $Gd_3Ga_5O_{12}$ (GGG) and yttrium oxide Y_2O_3 (YO) nanocrystals into the polymethyl methacrylate (PMMA) polymer matrix and the characterization of the synthesized materials by spectroscopic and emission dynamic studies are presented. The analyzed nanocrystals of YAG, GGG and YO compounds were prepared by the modified sol-gel method. The results indicate that the investigated materials, i.e. polymers with rare-earth containing oxide nanocrystals, can be useful for LSCs matched to the maximum sensitivity of a silicon EISC.

Key words: LSC, nanocrystal, luminescent center, EISC

Luminescencyjne koncentratory polimerowe zawierające nanokryształy tlenkowe domieszkowane wybranymi jonami ziem rzadkich dopasowane widmowo do krzemowych ogniw słonecznych oświetlanych krawędziowo

Streszczenie: Opracowano technologię luminescencyjnego koncentratora słonecznego (LSC) mogącego współpracować z nowego typu epitaksjalnymi ogniwami słonecznymi oświetlanymi krawędziowo (EISC). Przedstawiono zasadę działania i omówiono specyficzne cechy krzemowych ogniw typu EISC. Wskazano na potencjalne zastosowania w technologii LSC kompozytów aktywnych wytworzonych z wykorzystaniem nanokryształów luminescencyjnych wprowadzonych w matrycę polimerową (PMMA). Zsyntetyzowano przezroczysty kompozyt w wyniku wprowadzenia w matrycę z polimetakrylanu metylu (PMMA) nanokryształów granatu itrowo - glinowego $Y_3Al_5O_{12}$ (YAG), granatu gadolinowo – galowego $Gd_3Ga_5O_{12}$ (GGG) jak również tlenku itru Y_2O_3 (YO) domieszkowanych jonami Nd i Yb. Przedstawiono wyniki badań własności spektroskopowych nanokryształów otrzymanych zmodyfikowaną metodą zol-żel. Wyniki badań wytworzonych kompozytów polimerowych zawierających aktywne nanokryształy tlenkowe wskazują na możliwość ich zastosowania w luminescencyjnych koncentratorach słonecznych charakteryzujących się widmem fotoluminescencji dopasowanym do maksymalnej czułości widmowej krzemowego ogniwa krawędziowego.

Słowa kluczowe: LSC, nanokryształ, centrum luminescencyjne, EISC

1. Introduction

Solar cells, intended to transform sunlight into electricity, should meet local climatic conditions. The Central Europe weather is mostly cloudy and solar cells should utilize the scattered light for the most time. For this reason, flat solar panels without concentrators dominate this geographical region. However, luminescent light concentrators can work with the scattered light, thus being an alternative to the large area of flat silicon solar cells used in photovoltaic panels.

The luminescent concentrator is usually shaped in the form of a polymer plate or a film containing luminescent centers. The luminescent center absorbs the incident light and then emits the secondary photon oriented randomly in all directions inside the polymer plate. The photon emitted inside the concentrator material in the direction outside the cone of the internal reflection is guided inside the concentrator plate to the edge. Hence, the light emitted by the luminescent centers is guided and concentrated on the edge of the concentrator plate. The concentrated light may be utilized by PV cells coupled with the edge of the concentrator plate.

Therefore, the application of the LSC allows replacing some area of the semiconductor by cheap polymer plates in the construction of the planar PV panels.

In the first published experiments with LSCs [1 - 2] the laser dyes were used as luminescent centers suspended in the PMMA matrix. However, the main disadvantage of

the first LSCs was the poor stability of the available dyes. Also, the efficiency and absorption spectral range were not satisfactory. New, more stable perylene dyes, which became available at the beginning of the 21st century, offered new prospects for the development of the LSC technology [3 - 5].

It should be pointed out that the spectrum of light concentrated on the LSC edge differs from the sun spectrum because only the secondary photons emitted by luminescent centers can be guided to the edge. There should be a complete spectral separation between absorption and emission in the case of luminophores for the LSC. Hence, only a limited part of the sunlight spectrum can be utilized by the LSC. The absorption spectrum of perylene based dyes is limited to wavelengths shorter than about 700 nm. Taking into account that the silicon solar cell can convert the light having the wavelength of up to about 1000 nm, a significant part of the sunlight spectrum gets lost. This inevitable loss of the sunlight energy (even up to 45%) is considered the main disadvantage of the LSC concept.

The quantum dots (QDs) of II-VI semiconductor compounds or materials containing rare earth (RE) elements may be attractive alternatives to organic dyes. However, the efficiency of the II-VI QDs is far below expectations at the present level of technology [6]. Oxide nanocrystals doped with lanthanides suspended in the organic matrix were suggested in [5, 7 - 8] as a possible alternative to organic dyes.

The shape of the LSCs suggests the possibility of their coupling with slim and long PV cells. The edge-illuminated PV cell (EISC) proposed in the early 70s [9 - 11] seems to be well fitted to the LSCs requirements because of its geometry and spectral response. In this kind of a PV cell, the illuminated surface is perpendicular to the p-n junction and photons of any energy higher than the material bandgap are absorbed by the layer of the same thickness from the junction plane. Such PV cells are more sensitive at a long wavelength limit, when compared to the regular planar cells.

The new concept of the epitaxial EISC was proposed by our team and presented at the 24th and 25th EUPVSEC conferences. The epitaxial EISC was created in the form of the freestanding epitaxial silicon layer separated from the silicon substrate after epitaxial growth. All sublayers, including both p and n-type layers, were obtained during epitaxial growth [11].The unique spectral response of the EISC with the maximum near the long wavelength limit can be utilized if the energy of photons emitted by the LSC luminophore is just above the energy of the cell material bandgap. In order to make use of the unique properties of the epitaxial EISC we looked for suitable LSCs containing luminescent centers emitting photons of energy corresponding to the best spectral response of all the cells.

2. Epitaxial EISC

The epitaxial EISC units in the form of narrow strips were manufactured from multilayer epitaxial structures with p-n junctions located approximately in the middle of the structure. The epitaxial structure with a thickness of about 100 μm was separated from the substrate after epitaxial growth. and then chemically etched. The epitaxial EISCs were fabricated by cutting 0.1 mm thick free standing epitaxial foil into 40 – 60 mm long and 2 – 4 mm wide stripes. The area of the illuminated edge of the cell ranged from 0.04 cm^2 to 0.06 cm^2. So, the junction area was more than one order of magnitude larger than the illuminated area. As a result, the photocurrent density in the EISC across the junction was smaller than the photocurrent density in typical planar silicon cells. Fig. 1 shows the schematic presentation of an edge-illuminated solar cell made from silicon multilayered epitaxial structures [11]. The cells had a conversion efficiency in the 15 - 20% range, and the values of the fill factor (FF) reached about 0.6 – 0.68 when measured in laboratory conditions under

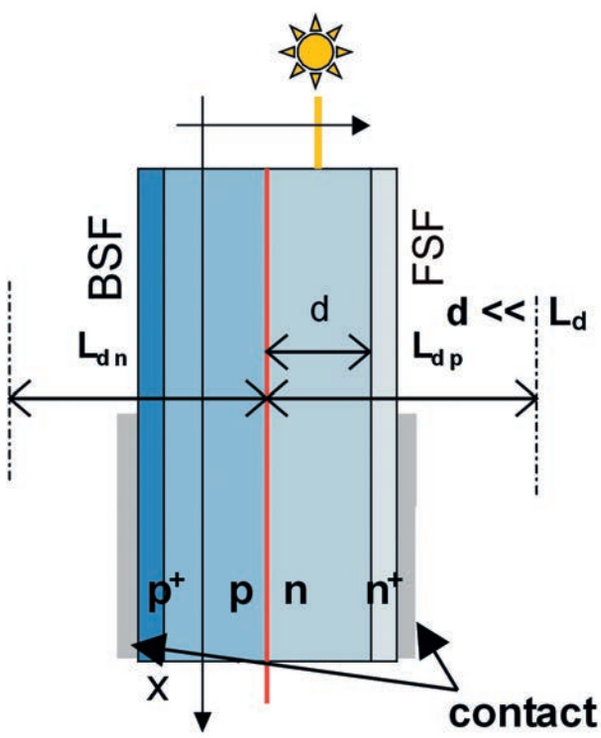

Fig. 1. Schematic presentation of a silicon EISC fabricated from a $p^+/p/n/n^+$ epitaxial structure. BSF and FSF denote Back Surface Field and Front Surface Field, respectively, d is the thickness of n and p-type epitaxial layers, and L_d is the diffusion length of minority carriers.

Rys. 1. Schemat ogniwa krawędziowego wykonanego z krzemowej struktury epitaksjalnej $p^+/p/n/n^+$, gdzie: BSF i FSF oznacza wbudowane pole wytworzone przez warstwę typu p^+ oraz n^+, d jest grubością warstw epitaksjalnych typu n i p oraz L_d jest długością drogi dyfuzji nośników mniejszościowych.

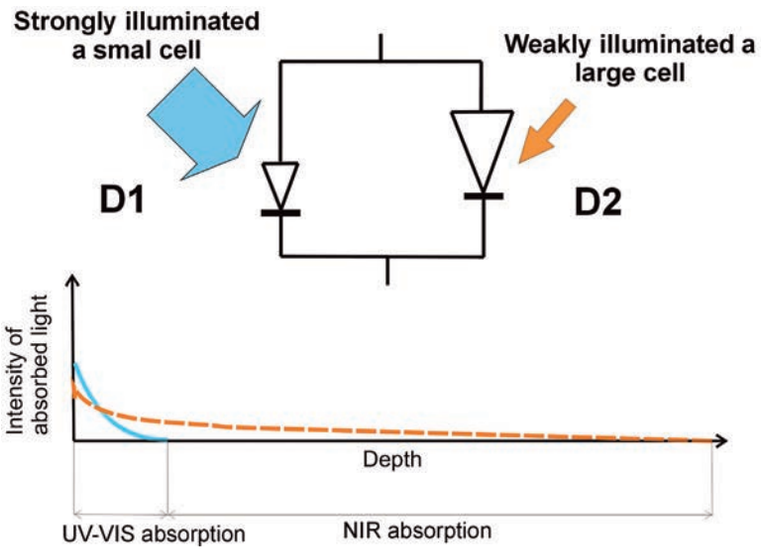

Fig. 2. The idea of a two cell model of an epitaxial EISC.
Rys. 2. Model dwuogniwowy epitaksjalnego ogniwa krawędziowego.

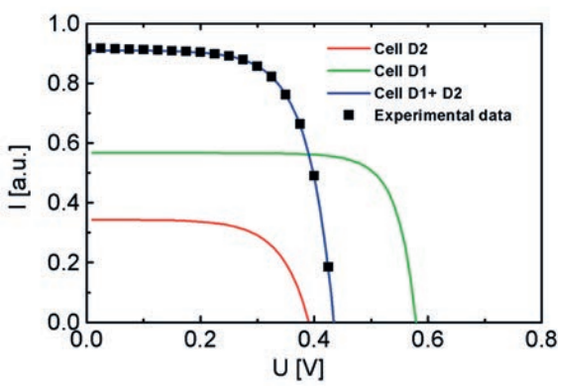

Fig. 3. Simulated I–V characteristics of D1 and D2 diodes compared to the recorded characteristic of an epitaxial EISC.
Rys. 3. Charakterystyki I-V diod D1i D2 uzyskane poprzez numeryczną symulację w zestawieniu z charakterystyką I-V epitaksjalnego ogniwa krawędziowego.

halogen lamp illumination. Simultaneously, it was found that the open circuit voltage Uoc was unexpectedly low and usually only slightly exceeded the value of 0.4 V [11].

The observed PV characteristics with a good efficiency and an unexpectedly low value of U_{oc} can be well simulated using a model consisting of two parallel, connected cells. One of them having a very small area and high illumination intensity represents the near surface region of the thickness of a few micrometers in which the UV visible and a short wave part of NIR (Near Infra-Red) light is absorbed. The second one with a large area and low illumination intensity represents the rest of the EISC of the thickness of about a few millimeters in which the photons of energy just over the band gap energy are absorbed (Fig. 2). Both cells are polarized with the same potential because the electric contacts are common. The resulting photocurrent is a sum of photocurrents generated in both cells. However, the U_{oc} value is diminished by the influence of the large area low illuminated cell as its I-V characteristic is only slightly shifted by the low density photocurrent. Taking into account that the ratio of both cell areas is about 10^2, and the ratio of the illumination level of these subcells is about 10^{-2}, the simulated I-V characteristics are in great accordance with the observed characteristics of the EISC, as shown in Fig. 3.

The surface recombination at the illuminated surface plays an essential role in the EISC PV characteristic. The recombination phenomena were observed as changes of the ideality factor value versus cell polarization after different types of mechanical and chemical surface treatment. After mechanical cutting, the ideality factor was extremely high and usually exceeded the value of 5 at about 0.3 V. The chemical surface finishing was developed so that the ideality factor value did not exceed 2 in the voltage range from 0.1 V up to 0.5 V, which indicates that the surface recombination effect on the I-V characteristics is negligible.

An edge-illuminated cell creates unique conversion conditions for photons with energy close to the band gap energy. Regardless of the depth of penetration into silicon, the incident photons are always absorbed in the layer of a constant thickness from the *p* - *n* junction limited by the thickness of the epitaxial structure only.

Taking into account that the thickness of the investigated EISC *n*- and *p*-type epilayers reaches about 0.05 mm and is essentially smaller than the diffusion length of minority carriers, the BSF layers at the external surfaces of both *n* and *p*-type layers can very effectively increase the number of photogenerated carriers which are passing through the *p*-*n* junction. The experimental data confirmed that the highest PV conversion efficiency was obtained for a relatively low doping level (10^{15} – 10^{16} cm^{-3}) of both p and n layers, which preserves the long minority carrier diffusion length.

Fig. 4 shows the internal quantum efficiency (IQE) of the typical planar c-Si cell and epitaxial EISC. The IQE

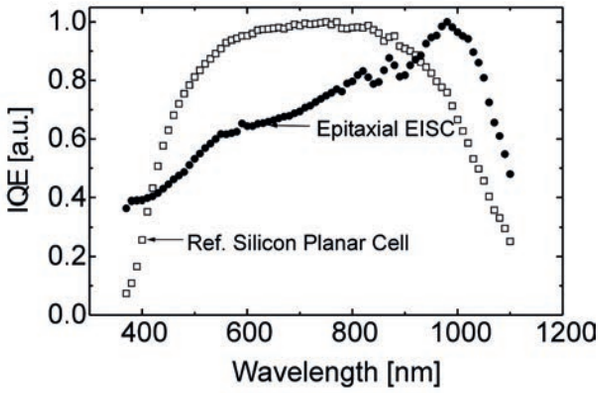

Fig. 4. Comparison of IQE of a reference silicon planar cell with the epitaxial EISCs.
Rys. 4. Porównanie charakterystyk czułości widmowej planarnego ogniwa krzemowego i epitaksjalnych ogniw krawędziowych.

maximum of the EISC is positioned at the wavelength of about 1000 nm and is shifted towards IR when compared to the conventional silicon planar PV cell. However, in the visible spectral range, the EISC efficiency is relatively lower. The EISC ensures favorable conditions for the conversion of photons absorbed in the cell at a distance from the surface much longer than the minority carrier diffusion length and therefore, should improve the efficiency of the EISC when compared to the planar cell for photons with energies slightly above silicon bandgap energy Eg. The diminishing observed for the EISC IQE in the visible spectral range is probably because of the recombination phenomena on the illuminated surface.

3. Selection of luminescent centers and preparation of LSCs

The spectroscopic properties of luminescent centers determine the parameters of LSCs. The luminescent species should possess a high luminescent quantum yield (LQY), high absorption coefficient, and low re-absorption losses (large Stokes shift). In recent years stable perylene dyes used for LSC doping have been developed. Unfortunately, the absorption range of these dyes is limited to about 600 nm. The maximum emission intensity falls at a wavelength of about 700 nm (see Fig. 9). The emission properties of the LSC containing perylene dyes do not ensure a good fit to the maximum spectral response of silicon.

The interaction between the LSC and silicon solar cells becomes the most efficient when the luminescent species absorb the sunlight up to the wavelength of about 900 nm and reemit in the spectral range of 950 – 1100 nm, which corresponds to the maximum sensitivity of the silicon solar cell. For this purpose, we consider using oxide nanocrystals doped with rare earth (RE) and transition metals (TM) ions as the active luminescent species for LSCs. Nanocrystals containing lanthanide ions offer a sufficient luminescent quantum yield and outstanding photostability. For the photovoltaic application, we choose garnet $Y_3Al_5O_{12}$ (YAG), $Gd_3Ga_5O_{12}$ (GGG) and Y_2O_3 (YO) nanocrystals co-doped with 3% Nd^{3+} and 15% Yb^{3+} ions and Y_2O_3 nanocrystals doped with ytterbium ions and sensibilized by Bi^{3+} ions. The Bi^{3+} ion is well known as an effective sensitizer for the Yb^{3+} ion in Y_2O_3 that results in enhancing the NIR emission of ytterbium [12].

Our previous study concerning the epitaxy and spectroscopic characterization of Nd,Yb:YAG waveguide structures for the NIR laser application showed that such RE ion system can be implemented in luminescent solar concentrators. The interaction between the neodymium ions absorbing solar radiation up to about 880 nm and ytterbium ions provides emission in the 900 – 1050 nm range. The highest efficiencies of energy transfer from neodymium to ytterbium were observed in Nd,Yb:YAG epitaxial layers for Nd^{3+} and Yb^{3+} ion concentration equal to 3 at. % and 15 at. %, respectively. This result determined a choice of the neodymium and ytterbium concentration in nanocrystals. For the Bi, Yb:Y_2O_3 nanocrystals, the Bi^{3+} concentration was established constant as 0.5 %, while the Yb^{3+} concentration varied reaching 1, 2 and 4 at. % in order to investigate the conversion efficiency versus the concentration ratio.

3.1. Synthesis of nanocrystalline powders

The co-doped YAG, GGG, and YO nanocrystals were prepared via the (Pechini) modified sol-gel method [13]. The preparation of the GGG, YAG and YO crystals is very similar. In the case of the GGG material both gallium and ytterbium oxide were dissolved in nitric acid. In the next step, gadolinium and neodymium oxides were dissolved in the solution of acetic acid. Both solutions were mixed together and stirred for 4 hours at 65°C with the addition of ethylene glycol as the cross-linking agent. The obtained mixture was dried at 120°C for 12 h and then ground in an agate mortar to fine the powder. This powder was calcined in the air at 1100°C. The synthesis of YAG or YO is less complicated because all starting oxides except Yb_2O_3 dissolve easily in acetic acid. The synthesis of YAG also requires the use of hydrated aluminum nitrate. The temperatures of YAG and YO calcination were 1000°C and 700°C, respectively.

The crystal structure of the obtained nanopowders, characterized by X-ray diffraction (XRD) using a Siemens D-500 diffractometer with CuKα radiation at 1.548 Å, was the single phase and had the crystalline structure as shown in Fig. 5. The mean size and morphology of nanocrystals analyzed by the Carl Zeiss AURIGA CrossBeam® Workstation scanning electron microscope (SEM) and evaluated using the Scherrer formula varied from 10 to 70 nm. The SEM image of the Nd,Yb:YAG, Nd,Yb:GGG and Nd, Yb:YO nanocrystals (Fig. 6) confirms that the nanopowders obtained by the sol-gel technique are fine – grained, but unfortunately agglomerated.

3.2. LSC preparation

As the first step, the nanopowders of Nd,Yb:YAG, Nd,Yb:GGG and Nd,Yb:YO were dried at 150°C in the air for 24 h. Next, the nanoparticles were deagglomerated ultrasonically directly in solvents, i.e. methyl methacrylate monomer /MMA/ or tetrahydrofuran (THF) in the presence of surface active agents. The following commercially available surfactants were used: Triton X-100, Dabco, Pluronic and dimethyldioctadecyl ammonium bromide (DDABr). The solution containing 0.2 g of nanocrystals per 100 cm^3 of the solvent with 0.1 ml or 0.05 g of the surface active agent (surfactant) per each 50 ml of the solution were prepared. The samples were ultrasonically treated with 50 kJ; 15/10 sec on/off duty cycle. The temperature of the samples was kept below 40°C to avoid the spontaneous polymerization of MMA. The size of nanoparticles was measured 1 hour after dispersion and repeated after 24 hours using MALVERN Instruments, Zetasizer, Model: Nano-ZS.1 and Malvern Dispersion Technology Software 5.10. The agglomerate size after the redispersion process was in the 10 nm - 100 nm range.

Two options were chosen for the LSC preparation: first - polymerization of MMA and second - dissolving polymethyl methacrylate (PMMA) pellets in THF and then drying. The MMA samples were mixed with luminescent nanoparticles and with 1% of Irgacure 1700 UV polymerization activator and then irradiated with UV light for 48 hours. The PMMA (PLEXIGLAS® 7N) pellets were dissolved in THF, dried in room conditions for 48 hours and then soaked at 60° C for 24 hours. The samples of polymer/nanocrystals composite with thickness in the 200 - 300 μm range were obtained.

The luminescence spectra were measured using the following monochromators: Spectra Pro 2300i (Princeton Instruments/ Acton) equipped with the thermoelectrically cooled InGaAs detector and HR 460 (Jobin-Yvon) with the photomultiplier R5509-72 (Hamamatsu) for the IR range. The emission decays were recorded with the TDS 2022B oscilloscope (Tektronix). The temperature stabilized laser diodes operating at λ = 808 nm and λ = 976 nm were used to excite Nd^{3+} and Yb^{3+} ions, respectively. For a direct excitation of Bi^{3+} ions a Cd – He UV laser emitting at λ = 325 nm was applied. The spectroscopic measurements were carried out both for nanocrystals and polymer composites. To measure the emission spectra of the LSC containing perylene dyes and PbS quantum dots, the Ar laser (λ = 488 nm) excitation was used.

4. Results and discussion

The single phase character and crystalline structure of all synthesized nanopowders were confirmed by the XRD measurements (Fig. 5). The mean size of the crystallites evaluated using the Scherrer formula varied from 10 nm to 70 nm.

The nanopowders of Nd,Yb:YAG\, Nd,Yb:GGG and Nd,Yb:YO produced by the sol-gel technique are fine--grained, but agglomerated as shown in the SEM image (Fig. 6). They require additional posttreatment to obtain homogeneous composites.

The best dispersion stability and optical quality of all polymerized samples was obtained with the DDABr surfactant for YAG nanocrystals and with Pluronic for GGG nanocrystals. The samples of Nd,Yb:YO were deagglomerated the same way as the garnet powders.

Polymer/nanosized particles luminescent composites were achieved via deagglomeration of nanocrystals and their subsequent incorporation into the PMMA matrix. Surfactants are needed for a better stability of dispersion.

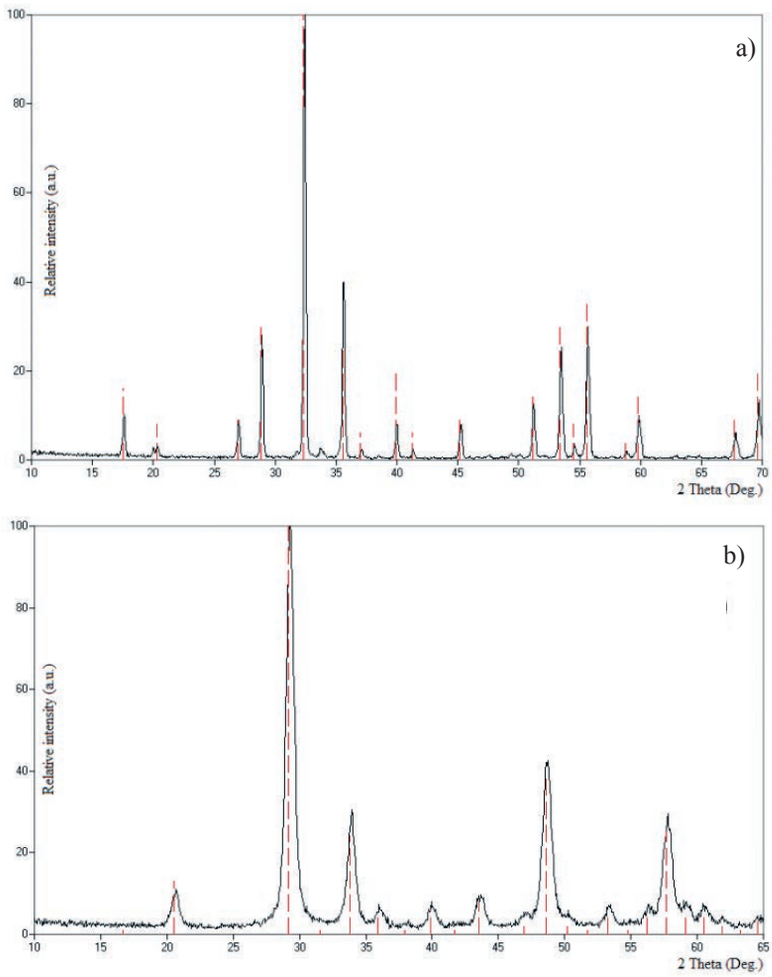

Fig. 5. X-ray diffraction patterns of nanopowders: (a) Nd,Yb:GGG and (b) Nd,Yb:YO.
Rys. 5. Dyfraktogramy nanoproszków o składzie: (a) Nd,Yb:GGG i (b) Nd,Yb:YO.

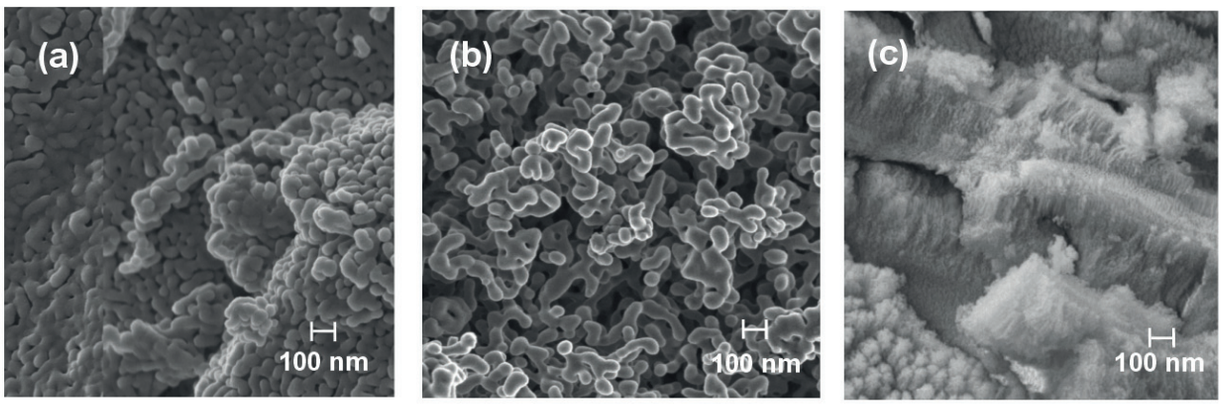

Fig. 6. SEM images of nanopowders: (a) Nd,Yb:GGG, (b) Nd,Yb:YAG and (c) Nb,Yb:YO.
Rys. 6. Obrazy SEM nanoproszków: (a) Nd,Yb:GGG, (b) Nd,Yb:YAG and (c) Nb,Yb:YO.

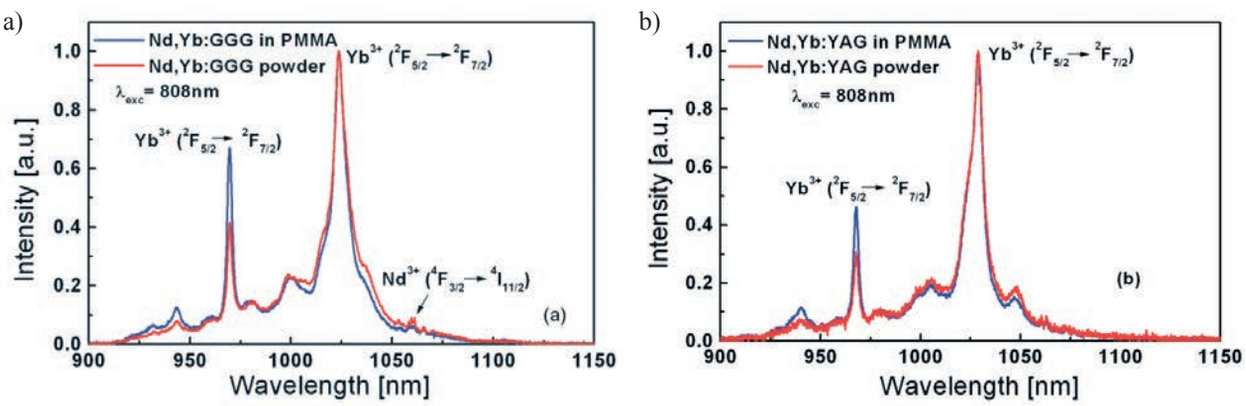

Fig. 7. Normalized emission spectra of Nd,Yb:GGG (a) and Nd,Yb:YAG (b) nanopowders as well as a sheet of the PMMA/nanocrystallites luminescent composite measured under 808 nm excitation.
Rys. 7. Znormalizowane widma emisji uzyskane w wyniku pobudzania promieniowaniam o długości fail 808 nm: nanoproszów (a) Nd, Yb: GGG I (b) Nd, Yb: YAG oraz nanokompozytu polimerowego PMMA/nanokryształy.

Ultrasonic treatment in ambient conditions seems to be efficient enough. After deagglomeration more than 90% (by weight) grains are less than 100 nm in size.

The surfactants used do not inhibit or influence the polymerization process. It should be noted that the physical and chemical properties of the polymer, like flexibility, hardness, and solubility are changed due to surfactant and nanocrystals incorporation but their influence on the physical properties must be studied separately.

Samples selected according to the abovementioned criteria were made for a higher nanocrystal concentration of 5% for YAG and 2.5% for GGG and with the higher thickness of 2 mm. The spectroscopic properties of the nanocrystals of YAG, GGG and YO co-doped with 3% Nd^{3+} and 15% Yb^{3+} ions were studied by means of photoluminescence and the time-resolved luminescence technique. All measurements were performed at room temperature. The IR emission properties of Nd,Yb:YAG and Nd,Yb:GGGnanopowders and polymer nanocomposites were investigated under quasi-CW 808 nm pumping, corresponding to the excitation of the $^4F_{5/2}$ level of Nd^{3+} ions. The luminescence spectra of 5 wt % of Nd,Yb:YAG in PMMA and 2.5 wt % of Nd,Yb:GGG in PMMA are shown in figures 7a and 7b, respectively. The luminescence signals attributed to active RE ions were detected at the edge of the LSC sheet.

The emission lines originating both from Nd and Yb ions are observed. Most of them can be attributed to transitions from the $^2F_{5/2}$ level in Yb^{3+} ions. The trace emission band centered at 1060 nm is related to the $^4F_{3/2} \rightarrow {}^4I_{11/2}$ transition of Nd^{3+} ion. This observation confirms the high efficiency of the energy transfer from neodymium to ytterbium ions.

Opposite to the garnet, in the Nd, Yb:Y_2O_3nanocrystalline powder, under 808 nm and 976 nm excitation, the observed IR luminescence signal was very weak. These observations are consistent with the results obtained for a singly doped oxide: Nd: Y_2O_3 [14] and Yb:Y_2O_3 [15]. In our measurements the lines of the Nd,Yb:YAG and Nd,Yb:GGG luminescence spectra in the wavelength region of 900 – 1100 nm were narrower compared with those of Nd,Yb:YO. For Nd,Yb:YO we observed broader lines due to the low phonon energy matrix [16].

The highest intensity of Yb^{3+} emission under 325 nm wavelength excitation was observed for the 2 at % concentrationof ytterbium ions (Fig. 8). The Yb^{3+} ions emission could only occur due to the energy transfer from Bi^{3+} ($^1P_1$) to Yb^{3+} ($^2F_{5/2}$) ions.

The broadband emission in the 400 – 600 nm range is attributed to the $^1P_1 \rightarrow {}^1S_0$ transition of Bi^{3+} ion (Fig. 8). The samples of Bi,Yb:YO nanopowders can absorb

a UV part of the solar light in the 300 – 400 nm rage and convert it into visible and infrared radiation useful for silicon solar cells.

The decay characteristics for the Nd,Yb:YAG and Nd,Yb:GGG nanopowders and composites of PMMA containing these luminescent species excited at 976 nm, were measured at room temperature. Regardless of the form of the measured samples, the decay characteristics and, of course, the lifetimes of the excited $^2F_{5/2}$ of the Yb^{3+} ion are almost the same. This observation confirms that PMMA does not change the spectroscopic parameters ofthe incorporated nanopowders.

A comparison of the luminescence spectra of LSCs containing different luminescence centers developed by our group is presented in Fig. 9. In the case of Nd, Yb:GGG and Nd,Yb:YAG nanocrystals, the spectrum of the absorbed sunlight is wider than for Bi,Yb:YO nanocrystals and the emission spectrum of the former corresponds to the absorption edge of silicon. The penetration depth of NIR radiation into silicon is much greater than that of the visible radiation emitted by Bi,Yb:YO (Fig. 8). Therefore, in contrast to the planar solar cells, the EISC performance is better in the NIR range. On the other hand, the radiation emitted by Bi,Yb:YO nanocrystals is more suitable for conventional silicon planar solar cells.

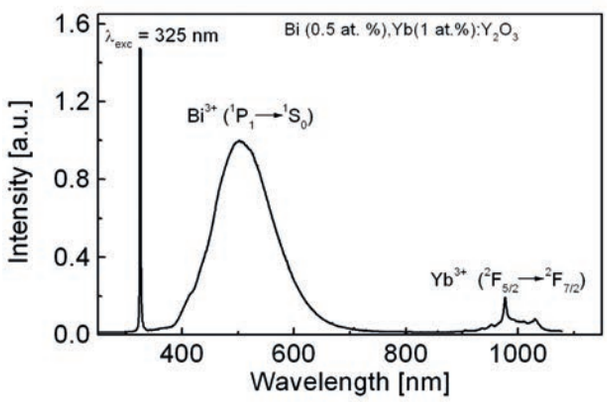

Fig. 8. Photoluminescence spectrum of Bi,Yb:YO nanopowder under excitation of Bi^{3+} ions at 325 nm wavelength.
Rys. 8. Widmo fotoluminescencji nanoproszku. Bi,Yb:YO przy wzbudzaniu jonów Bi^{3+} promieniowaniem o długości fali 325 nm.

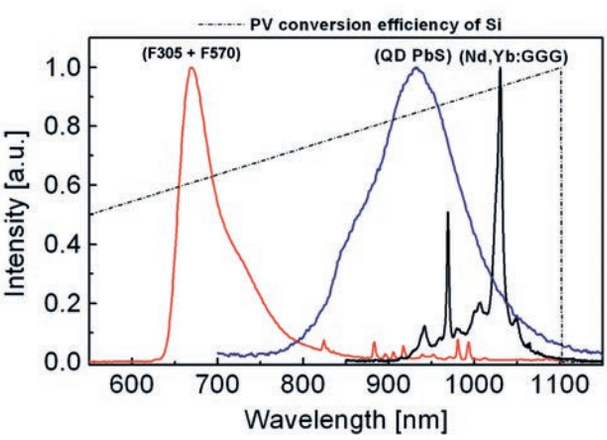

Fig. 9. Normalized emission spectra of PMMA doped with organic dyes (Lumogen F305 + F570), QD (PbS) and with Nd(3%), Yb(15%):GGG nanocrystals compared to c-Si conversion efficiency.
Rys. 9. Znormalizowane widma emisji luminescencyjnych koncentratów zawierających organiczne barwniki perylenowe (Lumogen F305 + F570), kropki kwantowe (PbS) oraz nanokryształy o składzie Nd(3%),Yb(15%):GGG w zestawieniu z sprawnością konwersji fotowoltaicznej monokrystalicznego krzemu..

5. Conclusions

The synthesis of the single phase nanocrystals of YAG, GGG and YO co-doped with neodymium and ytterbium ions in the 3 at. % and 15 at % concentrations respectively was successfully performed. Additionally, YO was doped with bismuth (0.5 at %) and ytterbium (1, 2, 4 at. %) ions. These dopants and their concentrations were chosen due to the efficient energy transfer between neodymium and ytterbium ions and from bismuth to ytterbium ions in order to reach emission in the spectral range matched to the best spectral response of a silicon solar cell. The samples obtained using the modified sol-gel method have satisfactory properties.

The synthesis of the transparent material by the incorporation of the clusters of Nd.Yb:YAG; Nd,Yb:GGG and Nd,Yb:YO nanocrystals into the PMMA polymer matrix was performed. The ultrasonic treatment seems to be an effective alternative to more advanced and sophisticated methods like the fluidized bed, rapid expansion from supercritical suspensions (RESS), stirring in the supercritical fluid at high pressures, using magnetically assisted impaction mixing (MAIM) and sonification in a supercritical fluid [17]. Taking into account that YAG and GGG show similar spectral properties, YAG appears more attractive due to more convenient dispersion properties.

The two methods of making the polymer matrix via bulk polymerization (MMA option) or drying from the PMMA/THF solution give flexibility and provide alternative ways for further technological development. However, in the THF option slightly finer-sized particles were achieved than in the MMA option.

These two methods do not produce differences in the spectral properties. The comparison between the spectral properties of nanocrystal powders themselves and nanocrystals embedded in PMMA shows that the polymer matrix does not change the spectroscopic properties.

The light emission with Yb ions in the oxide matrix with the wavelength close to the silicon absorption edge is well matched to the spectral response of EISC devices. Hence, the nanopowders with Yb ions can be considered as promising materials for the future LSCs.

It was found that the spectroscopic properties of Bi,Yb:YO nanopowders indicate the possibility of their use in the PMMA LSCs intended to work in conjunction with silicon PV cells. The LSC based on the composite PMMA - Bi,Yb:YO nanocrystals will be investigated.

Acknowledgments

The authors gratefully acknowledge dr M. Nakielska and dr A.Wnuk for the spectroscopic measurements. This work was partially supported by the Polish Ministry of Science and Higher Education under the research projects NN515518538, 742/N-POLONIUM/2010/0. and by the National Centre for Research and Development under the project GEKON2/04/266475/6/2015NR 15-0030-04

References

[1] Weber W. H., Lambe J.: Luminescent greenhouse collector for solar radiation, *Appl Opt.,* 1976, 15, 2299 - 2300

[2] Hermann A. M.: Luminescent solar concentrators - A review, *Sol. Ener.* 1982, 29, 323 - 329

[3] Tanaka N., Barashkov N., Heath J., Sisk W. N.: Photodegradation of polymer-dispersed perylene di-imide dyes, *Applied Optics*, 2006, 45, 3846 - 3851

[4] Kinderman R.; Slooff L. H.; Burgers A. R.; Bakker N. J., Büchtemann A., Danz R., van Roosmalen J. A. M.: I-V performance and stability study of dyes for luminescent plate concentrators, *Journal of Solar Energy Engineering*, 2007, 129, 277 - 282

[5] Rowan B. C., Wilson L. R., and Richards B. S.: Advanced material concepts for luminescent solar concentrators, *IEEE Journal of Selected Topics in Quantum Electronics*, 14, 2008, 1312 - 1322

[6] Pang L., Shen Y., Tetz K., Fainman Y.: Photosensitive quantum dot composites and their applications in optical structures, *Opt. Exp.,* 2005, 13, 44 - 49

[7] van der Ende B. M., Aarts L., Meijerink A.: Lanthanide ions as spectral converters for solar cells, *Phys. Chem*. 2009, 11, 11081 - 95

[8] Bünzli J. C., Eliseeva S. V.: Lanthanide NIR luminescence for telecommunications, bioanalyses and solar energy conversion, *J. Rare Ear.* 2010, 28, 824 - 842

[9] Hu C., Carney J. K., Frank R. I., New analysis of a high-voltage vertical multijunction solar cell, *J. App. Phys*. 1977, 48, 442 - 444

[10] Goradia C., Sater B. L.: A first order theory of the p^+-n-n^+ edge-illuminated silicon solar cell at very high injection levels, *IEEE Trans. on Electron Devices*, 1977, ED - 24, 342 - 351

[11] Sarnecki, J., Gawlik G. et al.: Concept of epitaxial silicon structures for edge illuminated solar cells, *Opt. El. Rev.* 2011, 19, 486 - 490

[12] Huang X. Y., Zhang, Q. Y. J.: Near-infrared quantum cutting via cooperative energy transfer in Gd_2O_3:Bi^{3+}, Yb^{3+}, Gd_2O_3:Bi^{3+},Yb^{3+} phosphors, *Appl. Phys*, 2010, 107 063505-063505-4

[13] Ryba-Romanowski W., Lipińska L., Lisiecki R., Rzepka A., Pajączkowska A.: Optical study of rare earth-doped $Gd_3Ga_5O_{12}$ nanocrystals obtained by a modified sol-gel method, *J. Nanos. and Nanot,* 2009, 9, 3020 - 3024.

[14] Walsh B. M., McMahon J. M., et al.: Spectroscopic characterization of Nd:Y_2O_3: application toward a differential absorption lidar system for remote sensing of ozone, *J. Opt. Soc. Amer. B*, 2002, 19, 2893 - 2903

[15] Shirakawa A., Takaichi K., Yagi H., Bisson J. - F., Lu J., Musha M., Ueda K., Yanagitani T., Petrov T. S., Kaminskii A. A.: Diode-pumped mode-locked Yb^{3+}:Y_2O_3 ceramic laser, *Opt. Express*, 2003, 11, 2911 - 2916

[16] Kozłowska A., Nakielska M., Sarnecki J., Lipińska L., Jeremiasz O., Podniesiński D., Maląg A.: Spectroscopic investigations of rare-earth materials for luminescent solar concentrators, *Opt. Appl.,* 2011, 41, 359 - 365

[17] Wei D., Dave R. N., Pfeffer R.: Mixing and characterizationofnanosized powders: an assessment of different techniques, J. *Nanopart Res*. 2002, 4:21- 41